GNPy: An open source application for physical layer aware open optical networks

# GNPy: an Open Source Application for Physical Layer Aware Open Optical Networks

ALESSIO FERRARI[1,*], MARK FILER[2], KARTHIKEYAN BALASUBRAMANIAN[2], YAWEI YIN[2], ESTHER LE ROUZIC[3], JAN KUNDRÁT[4], GERT GRAMMEL[5], GABRIELE GALIMBERTI[6], AND VITTORIO CURRI[1]

[1] DET, Politecnico di Torino, Corso Duca degli Abruzzi 24, Torino (TO), 10129, Italy
[2] Microsoft Corporation, Redmond, WA, USA
[3] Orange Labs, 22300 Lannion, France
[4] CESNET, Prague, Czech Republic
[5] Juniper Networks, Stuttgart, Germany
[6] Cisco Photonics, via S. M. Molgora, 48/C, Vimercate (MI), 20871, Italy
[*] Corresponding author: alessio.ferrari@polito.it

Compiled May 18, 2020

**In this article, we describe the validation of GNPy. GNPy is an open source application which approaches the optical layer according to a *disaggregated* paradigm and its core engine is a quality-of-transmission estimator (QoT-E) for coherent wavelength division multiplexed (WDM) optical networks. This software is versatile as it can be used to prepare a request for proposal/quotation in an RFP/RFQ process, as an engine of a what-if analysis on the physical layer, to optimize the network configuration maximizing the channel capacity and to investigate capacity and performance of a deployed network. We validate GNPy by feeding it with data from the network controller and comparing the results to experimental measurements on mixed-fiber, Raman-amplified, multi-vendor scenarios over the full C-band. We then test transmission distances from 400 up to 4000 km, polarization-multiplexed (PM) quadrature phase shift keying(QPSK), PM-8 quadrature amplitude modulation (QAM) and PM-16QAM formats, erbium-doped fiber amplifier (EDFA) and mixed Raman-EDFA amplification and different power levels. We show an excellent accuracy in predicting both the optical signal-to-noise ratio (OSNR) and the generalized signal-to-noise ratio (GSNR), within 1 dB accuracy for more than 90% of the 500 experimental samples. We also demonstrate the ability to estimate the transmitted power maximizing the GSNR within 0.5 dB of accuracy.** 

http://dx.doi.org/10.1364/ao.XX.XXXXXX

## 1. INTRODUCTION

Network operators are interested in maintaining the best performance of their optical networks and in identifying potential performance bottlenecks. However, currently, it is hard to have a unified vendor-neutral performance map of the optical network, because every vendor uses different performance prediction methods and performance indicators. This creates artificial barriers for operators, since expressing performance expectations in an RFP/RFQ process can become vendor dependent. What operators need is a tool to quickly model an optical network and run simulations in a vendor-neutral manner to properly match expectation with implementation. In particular, such vendor neutral simulation allows the seamless carryover of data from the past and from different vendors when modelling new networks. Breaking through the barrier, the Telecom Infra Project (TIP) open optical packet transport – physical simulation environment (OOPT-PSE) group [1] started in 2017 to define and develop a common, open source and vendor-neutral set of algorithms able to assess the optical impairments in an open optical line system.

The core software developed by the OOPT-PSE Team is called Gaussian noise simulation in Python (GNPy) [2] and relies on a quality-of-transmission estimator (QoT-E) which, given the network status, calculates the generalized signal-to-noise ratio (GSNR) [3] over a described network route. Furthermore, applications have been developed to describe [4], design [5, 6] and optimize [7, 8] optical networks based on it.In essence this allows a user to determine the feasibility of modulation and capacity allocation in fully coherent wavelength division multiplexed (WDM) networks with vendor-independent software. The computational time is a few seconds per lightpath (LP), with a target of well below one second per LP.

In past experiments, GNPy has been used with excellent

results in deployed networks, such as in 2017 [9, 10]. However those experiments were not validating the GNPy capability of QoT prediction on the entire C-band with Raman amplification, and did not benefit from a quasi-automatic procedure to provide input from the network controller directly to GNPy.

In this article, we extend the description in [11] by expanding the results obtained previously. We also provide a detailed description of the methodology to obtain reliable estimations from GNPy in a real network. In doing so, GNPy utilized the data structure provided by the network controller, including power levels measured by the on-board photodiodes and complemented it with data provided by the documentation of the devices such as the gain versus noise figure (NF) characterization of the amplifiers. Hence, this is the first validation of the entire process from the data collection through to the actual performance estimation and proves the feasibility of the GNPy integration in a network automation framework to enable operations such as path-computation for automatic ligthpath deployment and recovery. The validation process compared the estimated QoT, captured by the GSNR, against measurements.

The article is structured as follows. In section 2, we depict the general structure of GNPy and detail the core of GNPy: the QoT-E calculating the GSNR. In section 3, we describe the methodology used to validate the QoT estimation. This procedure can be also used as a guide to feed GNPy with the adequate network parameters. Then, in section. 4, we describe the test-bed and present the validation results. Finally, in section 5 we draw the conclusions and address future evolution.

## 2. GNPY: STRUCTURE AND IMPLEMENTATION

The general GNPy structure is illustrated in Fig. 1. GNPy provides a set of features structured around a core engine which takes care of propagation effects and the QoT estimation. The core engine is usually configured to simulate propagation of a fully loaded spectrum between points A and B in a complex topology. The network is built from atomic network *elements*, such as an erbium-doped fiber amplifier (EDFA), a fiber, etc., as described in more detail in section 2. As a result of the simulation, the core returns the GSNR [3] for each channel along the path. The GSNR has been proven as an effective unique metric for the QoT for modern coherent multilevel-modulated uncompensated WDM optical transmission [10].

More advanced features are handled by add-on modules which call out to the core engine for point-to-point QoT estimations.

To have meaningful GSNR results, GNPy requires a set of input parameters for each of the network elements along the path. In stable releases, these parameters are provided either in JavaScript object notation (JSON) format, or as a set of XLS files that are internally mapped into an equivalent JSON structure. Together, the parameters are used as inputs for the calculation of the amplified spontaneous emission (ASE) noise and of the non-linear interference (NLI) disturbance generated by the non-linear fiber propagation.

As a source of noise contribution towards the GSNR, the ASE noise depends strongly on the particular EDFA model. Amplifiers are described according to three general models [12] depending on the amount of knowledge of the amplifier:

1. A detailed white-box model that permits the user to define precise NF versus gain for open devices whenever the access to detailed performance is possible.

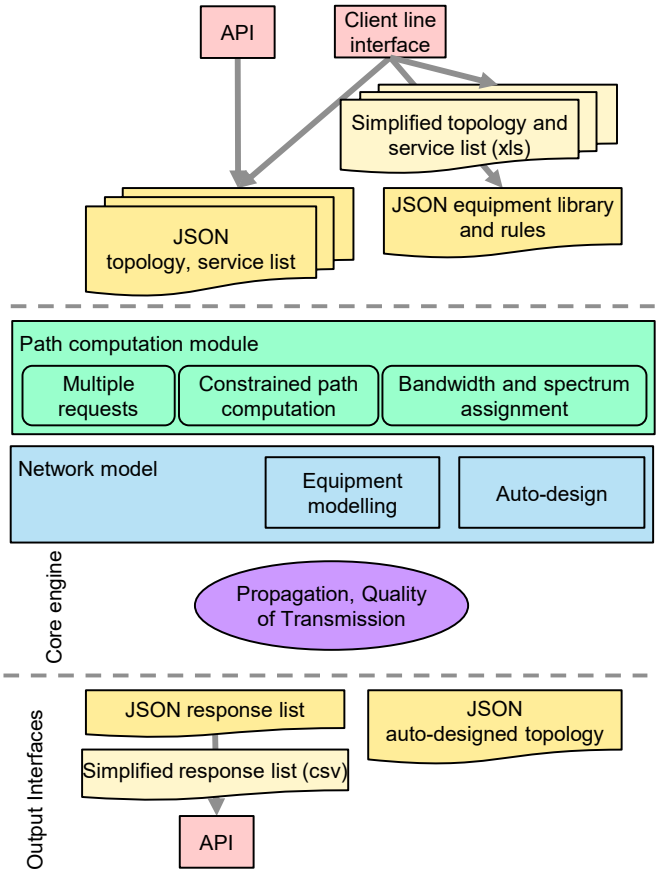


**Fig. 1.** GNPy general structure

2. An operator model that represents proprietary equipment for which knowledge is limited to a small amount of NF-gain values, available in data sheets.

3. A black-box model, for which key attributes such as internal output attenuation or switched gain range are not available.

This capability to support different amplifiers models is a key enabler for a multi-vendor application. Based on this equipment model a user can model a given green or brown field configuration provided that the whole set of equipment attributes is available.

There are scenarios when such a precise description is not available. For this reason, GNPy offers an *auto-design* feature capable to determine the amplifier configuration for a possible deployment on the basis of a set of design rules and heuristics. This practical implementation of optimization strategies is proposed in [12].

In auto-design mode, the input topology is not complete. The spans are not necessarily specified with all amplifiers, and the amplifier model and their operating points are not specified. Auto-design instead picks suitable amplifiers from the equipment library and it automatically splits long fiber spans.

A set of features eases the user experience for planning and what-if scenarios: it enables the propagation of multiple requests on the same simulated network, i.e., the same configuration of equipment. Typical planning constraints are supported such as path disjunction, mandatory nodes to be crossed, spectrum assignment and transponder mode selection, etc. This planning requires a third input from the user, listing the set of requests to

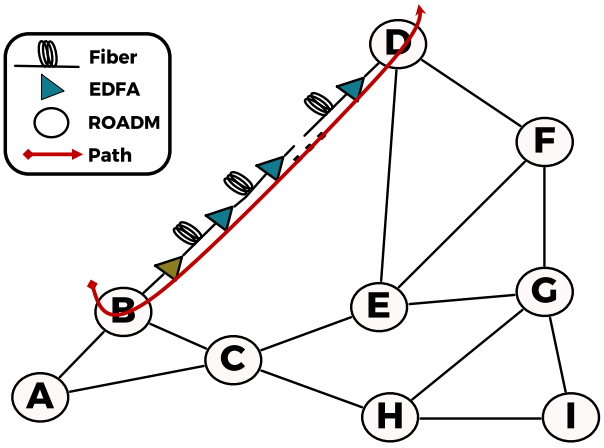


**Fig. 2.** Path propagation in GNPy to assess the QoT

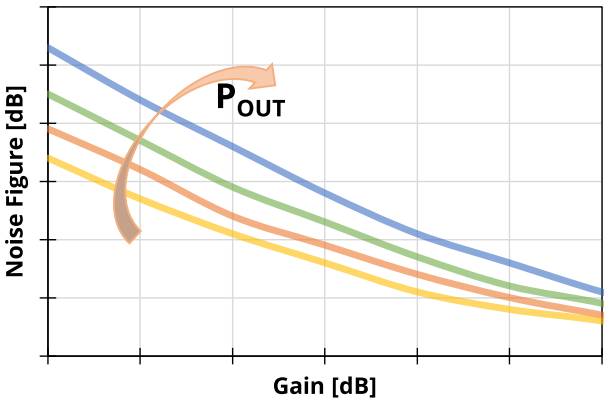


**Fig. 3.** Qualitative example of Noise Figure-vs-Gain and $P_{\text{out}}$ curves of an amplifier.

be evaluated with their constraints. The interface to this feature is a JSON file whose structure is inspired by [4]. This Path Computation Module enables the development of an application program interface (API) for the integration with optical line system controllers. For example, this API was recently featured at the 2019 TIP Summit in an open disaggregated transport network (ODTN) demonstration with the Czech Light Open Line System [13]. The path feasibility estimation has also been delegated to GNPy in Sodium-SR2 release of the TransportPCE controller project [14].

The QoT-E of GNPy requires a description of the network through a JSON file and it is abstracted as an optical impairment-aware topology [4, 15] (Fig. 2) in which, each *network element* is properly connected to the others, and it returns the GSNR for each channel at the end of a path. A network element can be a fiber, an optical amplifier, a ROADM node or a transceiver. Given this description of the physical layer, the GSNR between a source transceiver and a destination transceiver is assessed through the path under analysis by using the so called *spectral information*. The aim of the spectral information is to maintain all of the information related to the WDM comb such as the power of each channel, the roll-off, the symbol rate, the central frequency, the amount of ASE noise and NLI that affects that channel. Thus, such spectral information is generated by the source transceiver and it is *propagated* through each network element belonging to the path under analysis. These network elements update the spectral information by properly attenuating or amplifying each power value and by adding new ASE and NLI noise contributions on the spectral information if it is warranted. In particular, a ROADM node may add some noise in the add/drop channels and it equalizes the power per channel of the spectral information. The amplifier properly amplifies the spectral information and introduces some new ASE noise taking into account the possible frequency variation of the gain and the NF. The ASE noise power contribution, as a function of the frequency f, is computed as:

$$P_{\text{ASE}}(f) = hfNF(f)G(f)B_{ref}\,, \tag{1}$$

where $h$ is the Planck constant, $G(f)$ is the amplifier gain and $B_{ref}$ is the reference bandwidth in which the GSNR is evaluated. The fiber propagation attenuates the power levels and properly introduces the NLI generated by the Kerr effect taking into account also the stimulated Raman scattering (SRS) [16–19].

The SRS is assessed by implementing a *Raman solver* that numerically computes the solution of the set of ordinary differential equations (ODE) that describe the RS effect including also the two-point boundary value problem in the presence of counter-propagating Raman pumps, as shown in [20]. Thanks to the Raman solver, it is possible to assess the interchannel SRS, the SRS excited by the presence of co- and counter-propagating Raman pumps generated by Raman amplifiers, and also the spontaneous Raman scattering that is fundamental to assess the ASE noise generated by Raman amplifiers. Then, the NLI contribution of each fiber span is treated as an additive white Gaussian noise disturbance that takes into account the RS according to the generalized Gaussian noise (GGN) model [16–19], and this contribution is evaluated as:

$$P_{\text{NLI}}(f) = G_{\text{NLI}}(f)B_{ref}\,, \tag{2}$$

where, the $G_{\text{NLI}}(f)$ is the NLI power spectral density; it depends on the fiber parameters and on the WDM spectral occupancy. $G_{\text{NLI}}(f)$ is decomposed into self-channel interference (SCI), cross-channel interference (XCI) and multi-channel interference (MCI). While the SCI and the XCI are computed via the GGN model, the multi-channel interference (MCI) is not computed as it is negligible [21, 22]. This reduces the computational time as the complexity of the problem moves from quadratic with respect to the number of channels to linear. Finally, the transceiver at the end of the path receives the spectral information and returns the propagation performances of each channel by computing the GSNR that includes both the optical signal-to-noise ratio (OSNR) and the non-linear signal-to-noise ratio ($\text{SNR}_{\text{NL}}$). Those quantities are defined and computed on the $i$-th channel as:

$$\text{OSNR}_i = \frac{P_{S,i}}{P_{\text{ASE}}(f_i)}\,, \tag{3}$$

$$\text{SNR}_{\text{NL,i}} = \frac{P_{S,i}}{P_{\text{NLI}}(f_i)}\,, \tag{4}$$

$$\text{GSNR}_i = \frac{P_{S,i}}{P_{\text{ASE}}(f_i) + P_{\text{NLI}}(f_i)} = \left(\text{OSNR}_i^{-1} + \text{SNR}_{\text{NL,i}}^{-1}\right)^{-1}\,, \tag{5}$$

where $P_{S,i}$ is the signal power of the $i$-th channel and $f_i$ is its central frequency.

## 3. VALIDATION METHODOLOGY

The aim of this validation is to prove the capability of GNPy to predict the GSNR of real commercial line systems, relying

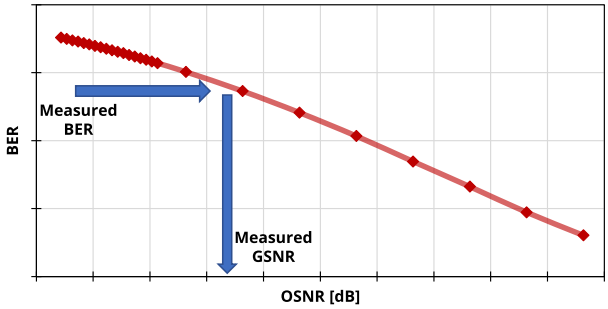


**Fig. 4.** Qualitative example of B2B BER-vs-OSNR response of the transponder and derivation of GSNR from a BER measurement.

only on data provided by the network equipment, such as the power levels measured by the on-board photodiodes and the parameters provided by the documentation of the devices such as the gain-versus-NF characterization of the EDFAs. Hence, in this section, we describe this process that leads to the building of the JSON describing ROADM nodes, fibers and amplifiers.

Each ROADM node requires a target output power per channel that can be retrieved from the total power measured by the photodiode before the booster amplifier divided by the number of channels. Then, each amplifier requires a gain target and a tilt target, and this information can be provided by the network equipment and can be retrieved with a representational state transfer (REST) [23] query (or other methods such as using network configuration protocol (NETCONF) [24] directly on the equipment can be adopted). Furthermore, the amplifier NF has to be derived to properly assess the ASE noise level. To do this, the data model of GNPy for EDFA is fed with the gain-vs-NF characterization from the documentation of the amplifier; as this curve depends also on the input power, it is necessary to use the proper curve depending on the output power ($P_{\text{out}}$) level that is measured by the amplifier photodiode. A qualitative example of NF-vs-gain and $P_{\text{out}}$ characterization is shown in Fig. 3. The values in Fig. 3 are for illustration purpose only and not from any real amplifier.

To describe a fiber span, it is necessary to input the fiber type, the fiber length ($L_F$), the attenuation coefficient ($\alpha$) and the connector losses. Furthermore, when Raman pumps are injected into the fiber by Raman amplifiers, the parameters related to the Raman pumps and the temperature of the fiber are also needed. The fiber types already available in GNPy are: standard single mode fiber (SSMF), non zero dispersion shifted fiber (NZDSF), large effective area fiber (LEAF), but it is also possible to define custom fiber types. To define a custom fiber type it is enough to know the dispersion, the non-linear coefficient and the Raman efficiency. The length $L_F$ can be retrieved by computing the distance between the locations of the amplification sites or it can be obtained by the network equipment by measuring the propagation time between two amplifiers. For each fiber type we use the specified attenuation coefficient from the data-sheet. Then, the connector losses can be estimated knowing the overall span loss ($A_s$): it can be derived by computing the difference between the total power measured by photodiodes placed at the output of the previous amplifier and at the input of the following amplifier. Thus, the overall splice-plus-connector loss ($A_c$) can be derived knowing $A_s$ and the fiber loss ($A_F$):

$$A_c = A_s - A_F = A_s - \alpha \times L_F \ . \tag{6}$$

Then, the proper partition of this loss is crucial as the input connector loss determines the amount of NLI generated by that fiber span. As the optical time domain reflectometer (OTDR) trace is not always available, it may be impossible to retrieve the concentrated loss distribution along the fiber. For this reason it is necessary to make some assumptions: for the input connector loss we use 0.75 dB as it is a typical value reported in [25] and was used in [10, 26]. The residual loss is then concentrated in the output connector loss even if the actual loss is distributed along the fiber because of the various splices. The fiber temperature, if not known, can simply be assumed equal to the 295 K room temperature.

Finally, the Raman pumps are described by their frequency and their power. The pump frequency is provided by the documentation, while the value of each transmitted pump power can be obtained from a REST query to the Raman amplifier. To properly derive the actual power of the pumps injected into the fiber, it is necessary to subtract the concentrated loss between the pump sources and the fiber. This value can be obtained by querying the OTDR situated on each Raman card.

By following this procedure for all the network elements, it is possible to complete the description of the topology and GNPy can compute the QoT of a path in the network. We want to specify that, in this procedure, the auto-design feature is not used.

In order to verify the accuracy of the estimation it is necessary to measure the GSNR. We do it querying the bit-error-rate reported by the transponder and inferring the corresponding measured GSNR by inverting the back-to-back (B2B) BER-vs-OSNR characterization of the transponder as qualitatively shown in Fig. 4. The values are not shown due to nondisclosure agreements with the manufacturer. We performed this procedure for each transceiver for each modulation format. Finally, the error is computed as the difference between the measured GSNR and the one estimated by GNPy. We also observe the accuracy in predicting the OSNR by using the built in functionality of the optical spectrum analyzer (OSA). As shown in [27], the signal and ASE noise power are estimated by using an OSA. In particular, the ASE noise is estimated by measuring it at the left and at the right side of the channel and averaging the two measurements.

## 4. VALIDATION

In this section we describe the test-bed used in Microsoft labs and report the validation results.

### A. Test-bed Description

The test-bed used for the experiments is shown in Figs. 5: it emulates a commercial network with six ROADM nodes and five amplified optical segments and the longest bidirectional path in the network is 2000 km long. The transponders come from three different vendors, whereas all the ROADM nodes and the amplifiers originate from a fourth vendor. Each node degree of each ROADM node has a booster amplifier and a pre-amplifier. Each line segment is roughly 400 km long, and it includes four in-line amplifiers (ILA): three lumped EDFAs and one hybrid Raman-EDFA amplifier with Raman amplification operating in the moderate pumping regime [28]. The length of the fiber spans varies from 65 km to 120 km, and the fiber types are G.652 standard single mode fiber (SSMF) and G.655 LEAF fiber. The exact network topology, the detailed length of each fiber span, the fiber type and the position of each EDFA and Hybrid Raman-EDFA amplifier are shown in Fig. 5a. The line

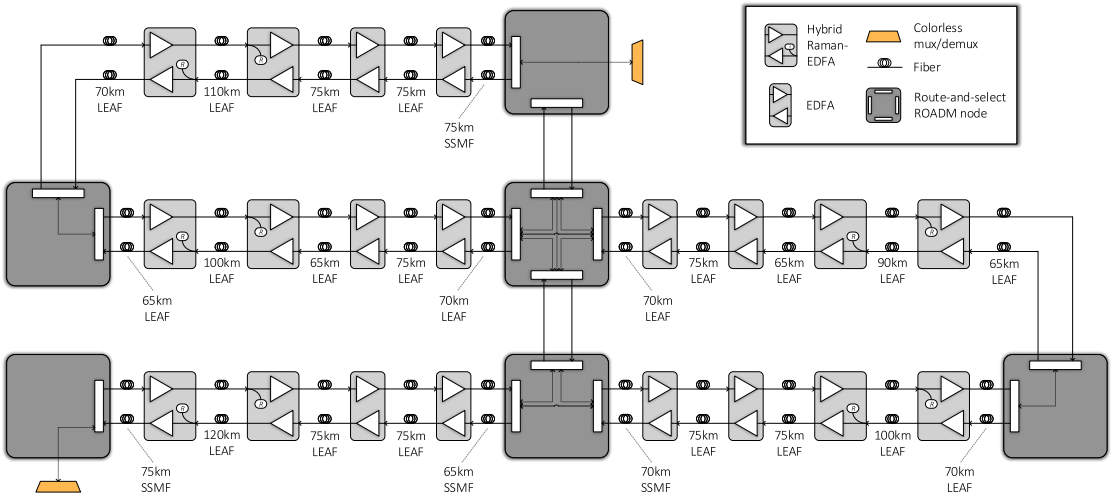


**(a)** Block scheme of the Microsoft test-bed.

**(b)** A photo of the Microsoft test-bed.

**Fig. 5.** The block scheme (a) and a photo (b) of the Microsoft test-bed.

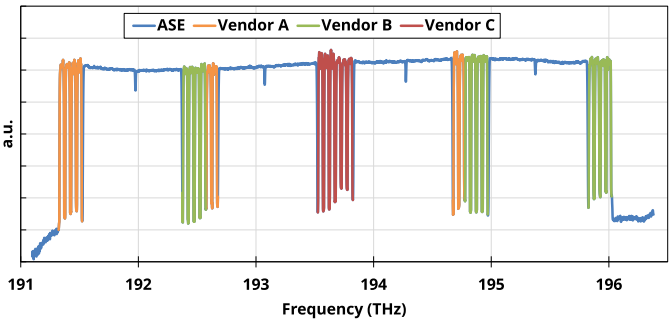


**Fig. 6.** Transmitted spectrum. Channels of different vendors are reported with different colors.

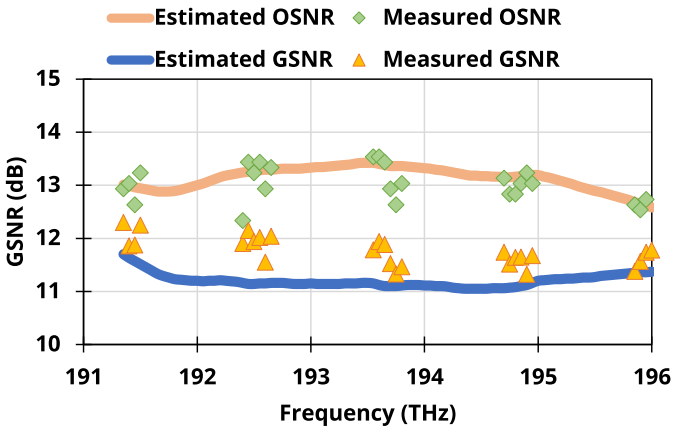


**Fig. 7.** Comparison of measured and estimated OSNR and GSNR from PM-8QAM @ 2000 km

system has been properly configured by a vendor proprietary controller. In order to collect and prepare the information, as described in section 3, the state of the network was probed by querying it via Microsoft software defined network (SDN) line system monitoring tool, which is based on REST.

The normalized transmitted spectrum, shown in Fig. 6, is transmitted and received through the colorless mux/demux. Its bandwidth occupation is 4.7 THz, from 191.325 THz up to 196.025 THz. Commercial multi-vendor coherent transponders from three different vendors are used to generate a total of 26 channels under test (CUT) grouped into five media-channels (MC). Two MCs are comprised of four channels, and the remaining three MCs are made of six channels. The WDM grid spacing is 50 GHz and the MCs are distributed in the spectrum as follows: the two four-channel MCs are positioned at the edges of the spectrum, with one six-channel MC in the middle and the remaining two MCs are in the midpoints between the central MC and the external MCs. The rest of the spectrum is filled with properly shaped ASE noise in order to obtain a full C-band spectral load, as shown in [29]. The signals are root-raised cosine shaped with a roll-off of 0.2 and the symbol rate is 34.16 GBaud. The transponders support three modulation formats: PM-QPSK, PM-8QAM and PM-16QAM. We tested different modulation formats and propagation distances: PM-QPSK at 2000 km and 4000 km, PM-8QAM at 400 km, 800 km, 1200 km, 1600 km and 2000 km and PM-16QAM at 400 km, 800 km and 1200 km, both in forward and in backward directions. The 4000 km path was obtained by looping back the signals over the 2000 km path. Finally, we also tested PM-8QAM along the 2000 km path in both directions without Raman amplification. To do this, we turned off all the Raman amplifiers in all hybrid Raman-EDFA amplifiers and we set the gain of the EDFA to compensate for the absence of Raman gain.

### B. Results

The validation demonstrates that the tool effectively predicts both the OSNR and the GSNR with excellent accuracy, and further, it is able to accurately capture the frequency variation of both metrics. The first observed case is the 2000 km forward direction with PM-8QAM modulated CUTs - shown in Fig. 7. Both the OSNR and the GSNR are measured (diamond and triangular markers, respectively) and compared to the estimates (continuous lines). The OSNR was measured with an OSA, while the GSNR has been measured by reading the BER from the cards and by inverting the B2B characteristic of each card as discussed in Section 3. This first result demonstrates good accuracy in the estimates of both the OSNR and the GSNR. It can be noted

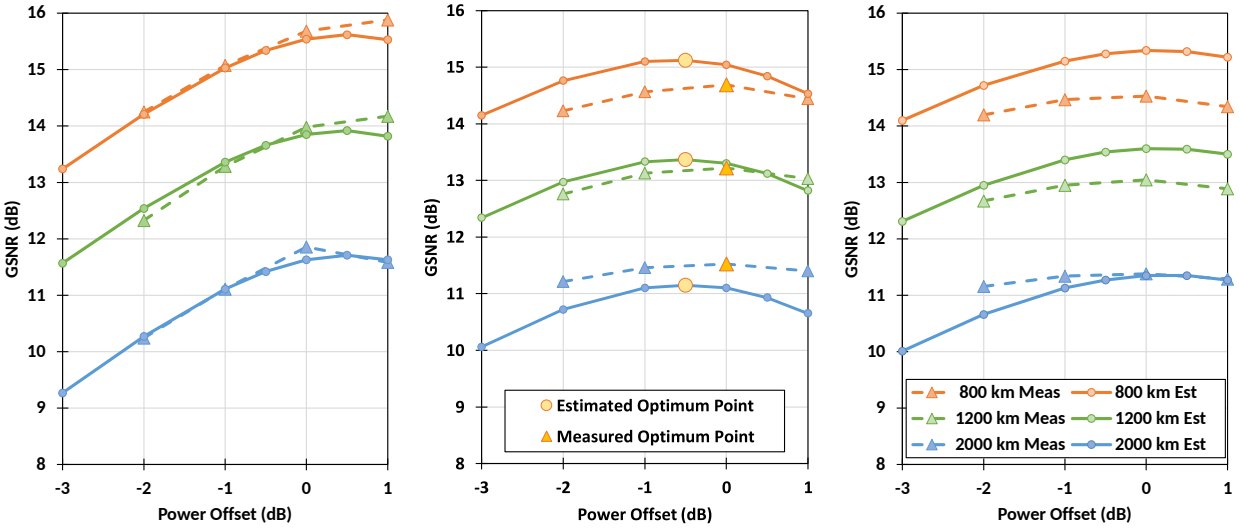


**(a)** Channel #2 at 191.4 THz. **(b)** Channel #48 at 193.5 THz. **(c)** Channel #92 at 195.9 THz.

**Fig. 8.** Comparison of estimated and measured GSNR in a power sweep for PM-8QAM. The legend shown in (c) applies to all three graphs.

that the estimated OSNR has an error within 0.4 dB except one outlier at 192.4 THz and at 193.75 THz. In this case, GNPy shows an excellent capability in predicting the frequency variation of the two metrics and a conservative estimation of the GSNR as expected by the GGN model for which estimation of the NLI is worst case. Here, the discrepancy between the measured GSNR and the estimated one is within 1 dB.

Moreover, we performed a power sweep, i.e., we varied the transmitted power at the beginning of each optical line by a power offset from -3 dB up to +1 dB. Figures 8 report the results of the power sweep as a comparison of the measured and the estimated GSNR for channels #2, #48 and #92 - at 191.4 THz, 193.5 THz and 195.9 THz -, i.e., two at the edges and one in the middle of the spectrum, at 800 km, 1200 km and 2000 km. The results show a good accuracy in predicting the GSNR as well as the optimum power, i.e., the one maximizing the GSNR of the central channel as shown by the local-optimum global-optimum (LOGO) approach [30]. The predicted optimum power is always within 0.5 dB of the measured optimum. This demonstrates the accuracy of the tool in estimating the optimum power and thus, it can be integrated into an optical controller to optimize the transmitted power.

Figures 9, 10 and 11 report the estimated GSNR (blue lines) and the measured one (orange dots) for all the investigated scenarios with PM-8QAM, PM-QPSK and PM-16QAM modulation formats respectively. Each of them has been reported for several distances and for both directions. Furthermore, Figs. 12 report the results when the Raman amplification is turned off. The QoT-E shows good accuracy in the estimation showing a small discrepancy with respect to the measured values and demonstrating good capability in predicting the frequency variation of the GSNR. Moreover, as the QoT-E is based on the GGN model, it neglects the impact of the modulation format on the NLI generation. For this reason, the QoT-E predicts the same GSNR for the same distance and direction when only the modulation format changes and, as expected, this assumption is validated as the modulation format has a negligible impact on the measured GSNR. Observing the shorter 400 km distances, in Figs. 9a, 9f, 11a and 11d a larger inaccuracy is present in the middle of the band. Increasing the distance this error reduces since the overall GSNR reduction mitigates the uncertainty on both ASE noise and NLI. For shorter distances, in fact, it is more difficult to accurately measure the GSNR as i) the BER is lower, then, less stable as, in the measurement time window, less errors are counted, ii) the GSNR itself is higher and therefore more sensitive to small inaccuracies. For shorter distances, in fact, the noise power is smaller and thus, each inaccuracy has a larger effect in the overall GSNR. For the same reason, the B2B characterization is also less accurate where the BER is lower and the OSNR is higher, making the measurement less accurate.

Finally, the estimated GSNR shows excellent accuracy when the Raman cards are turned off, as shown in Fig. 12, demonstrating that the QoT-E can be used also as an engine for what-if investigations in a techno-economic analysis to understand whether it is advantageous to use Raman amplifiers to improve the GSNR of a network.

Finally, the error of each channel in each scenario has been computed as the difference between the measured GSNR and the estimated GSNR (i.e., Measured GSNR – Estimated GSNR). This set of errors has more than 500 values. Figures 13 report the error distribution for each distance (Fig. 13a) and for each modulation format (Fig. 13b) as a box-plot. The distributions looks quite symmetric with a positive offset of ∼0.25 dB. ∼80% of the estimations are within 1 dB of error at 400 km. This percentage increases to ∼92% at 800 km; it reaches the 100% for larger distances. The largest error is at 400 km and it is 1.4 dB. This value reduces at larger distances, and all the errors are within 0.5 dB at 4000 km. The average and the median error is ∼0.5 dB at 400 km and 800 km, then it oscillates around 0.4 dB and 0.3 dB when the distance increases to 1200 km and 2000 km. Finally, the value shrinks down to 0.2 dB when the reach is 4000 km. Figure 13b shows the error distribution for each modulation format. The PM-QPSK exhibits the smallest error distribution, whereas PM-16QAM exhibits the largest inaccuracy. The average and the median error are roughly 0.2 dB for the PM-QPSK, 0.4 dB for the PM-8QAM and 0.5 dB for PM-16QAM. This is because PM-QPSK has been measured at the largest distances, were the accuracy is better, while PM-16QAM has

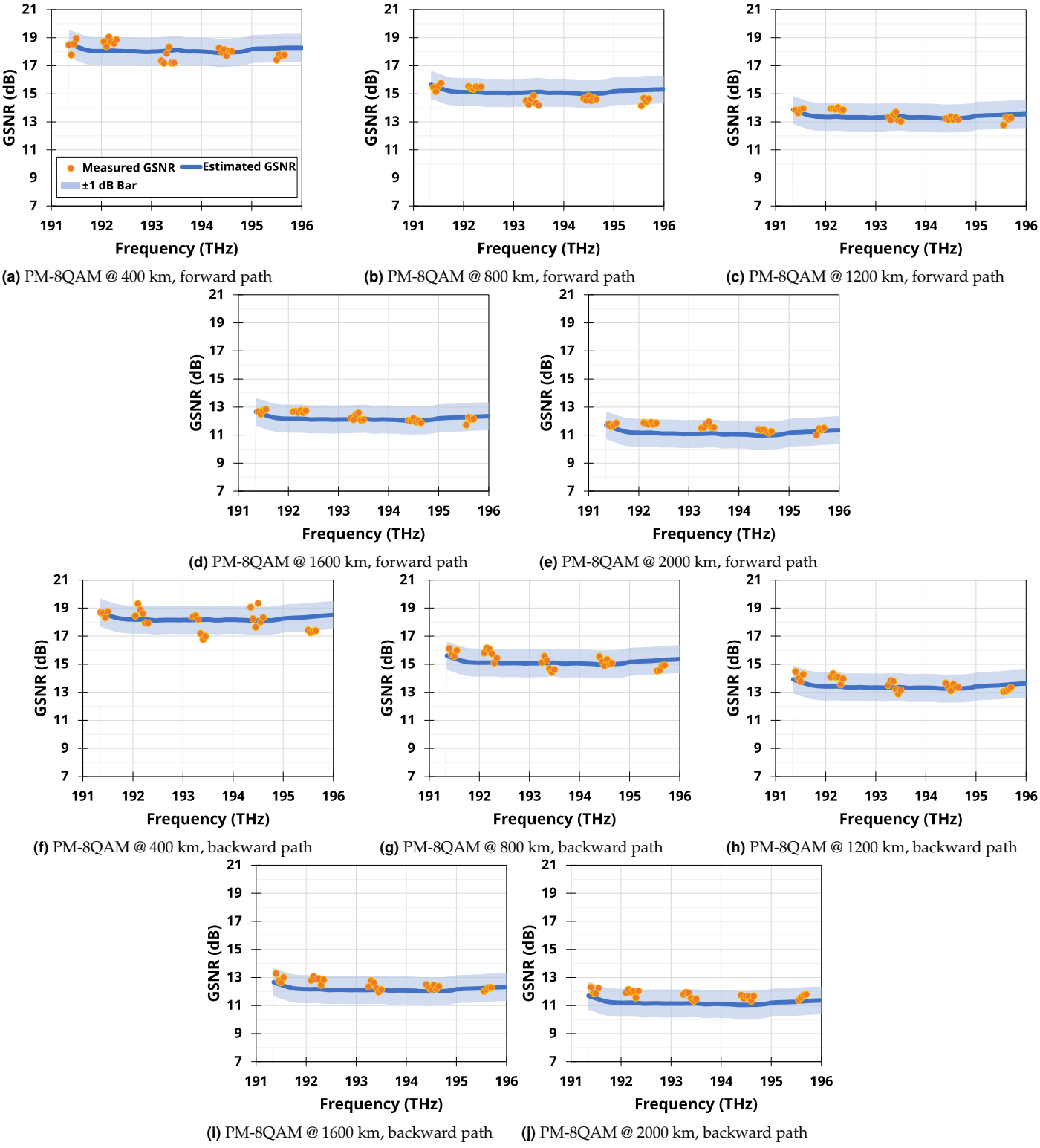


**(a)** PM-8QAM @ 400 km, forward path

**(b)** PM-8QAM @ 800 km, forward path

**(c)** PM-8QAM @ 1200 km, forward path

**(d)** PM-8QAM @ 1600 km, forward path

**(e)** PM-8QAM @ 2000 km, forward path

**(f)** PM-8QAM @ 400 km, backward path

**(g)** PM-8QAM @ 800 km, backward path

**(h)** PM-8QAM @ 1200 km, backward path

**(i)** PM-8QAM @ 1600 km, backward path

**(j)** PM-8QAM @ 2000 km, backward path

**Fig. 9.** Comparison of estimation with measurement for PM-8QAM

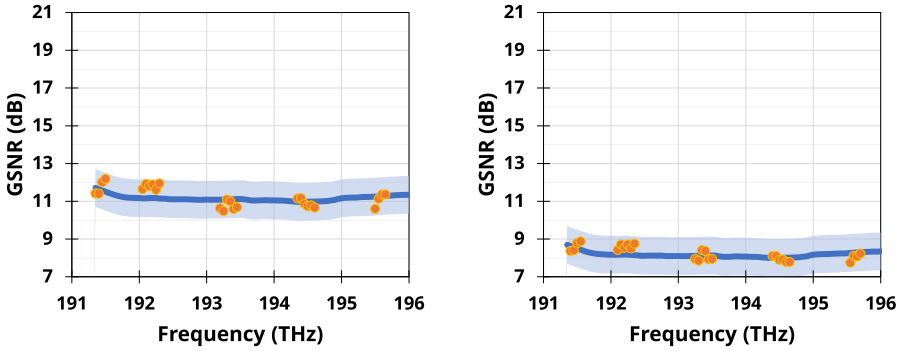


**(a)** PM-QPSK @ 2000 km, forward path **(b)** PM-QPSK @ 4000 km, loop-back

**Fig. 10.** Comparison of estimation with measurement for PM-QPSK

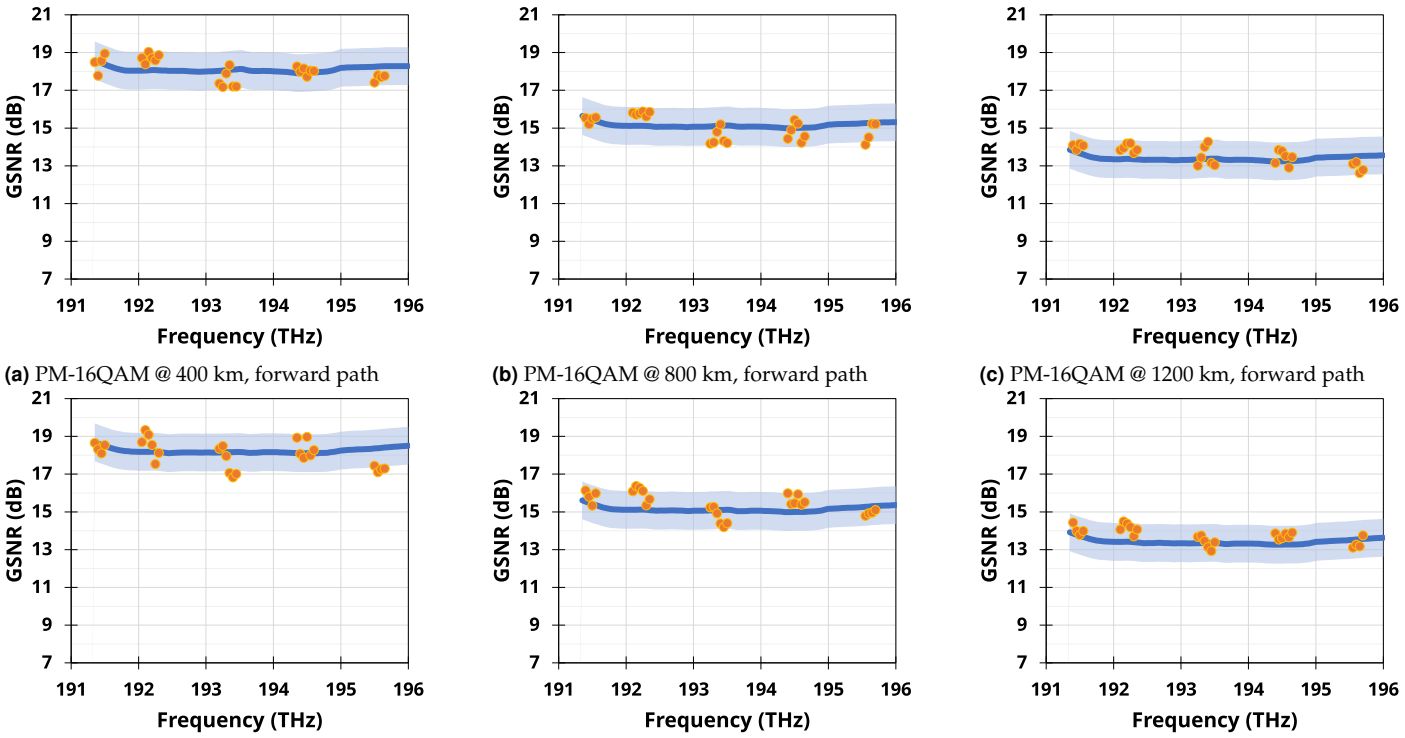


**(a)** PM-16QAM @ 400 km, forward path **(b)** PM-16QAM @ 800 km, forward path **(c)** PM-16QAM @ 1200 km, forward path

**(d)** PM-16QAM @ 400 km, backward path **(e)** PM-16QAM @ 800 km, backward path **(f)** PM-16QAM @ 1200 km, backward path

**Fig. 11.** Comparison of estimation with measurement for PM-16QAM

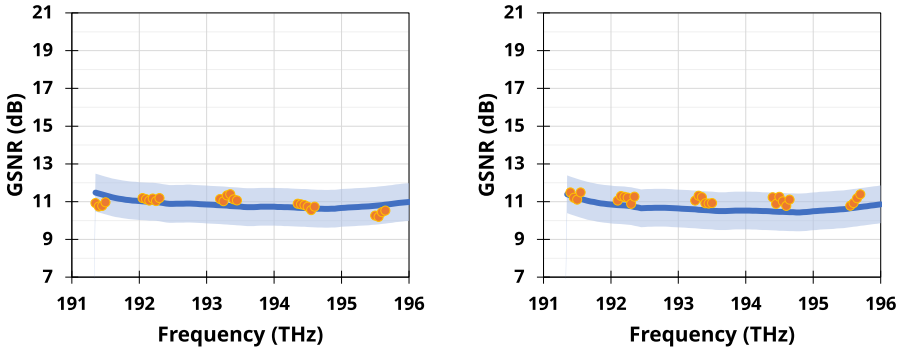


**(a)** PM-8QAM @ 2000 km, forward path **(b)** PM-8QAM @ 2000 km, backward path

**Fig. 12.** Comparison of estimation with measurement for PM-8QAM with Raman amplifiers turned off.

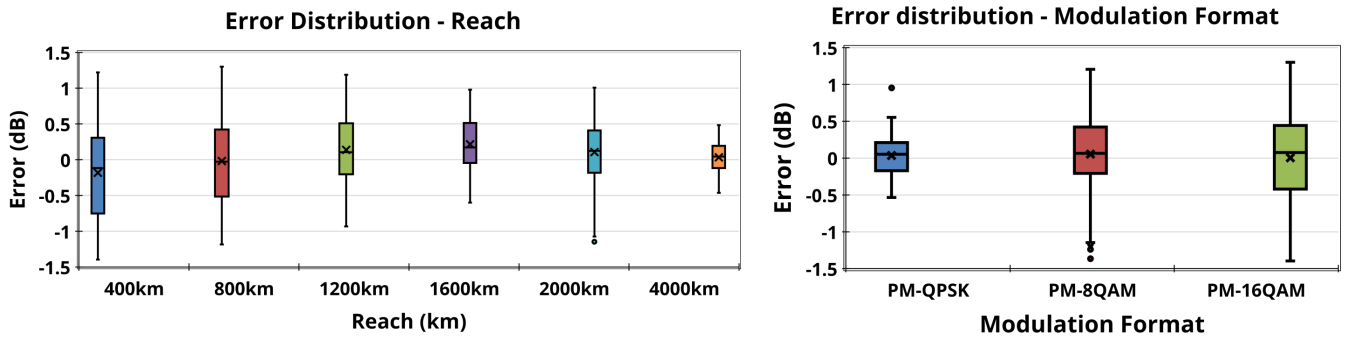


**(a)** Error distribution versus reach.

**(b)** Error distribution versus modulation.

**Fig. 13.** Error distribution with respect to the reach and the modulation format.

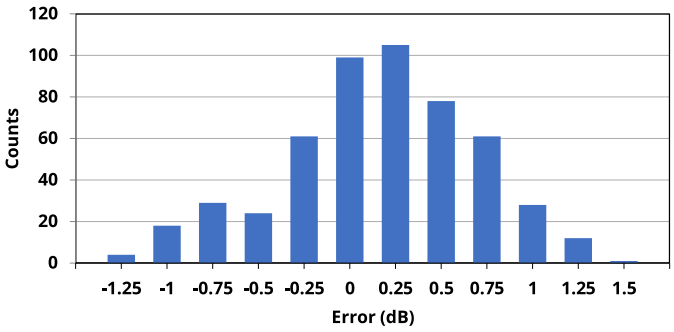


**Fig. 14.** Error histogram over all measured points.

been probed at the shortest reaches of 400 km, 800 km and 1200 km. Finally, Fig. 14 reports the error distribution. 90% of the errors are smaller than 1 dB. Moreover, the distribution is not symmetric around 0, in fact, 74% of the errors are positive and the largest value is 1.4 dB. This means that most of the estimations are conservative. The error is due to three main factors: (i) the conservative assumptions on which the GGN model is based, (ii) the uncertainty in the measurement of the GSNR and (iii) the inaccuracy in measuring the parameters provided to GNPy to compute the estimated GSNR. In particular, factors (ii) and (iii) can lead to a non-conservative estimation of the overall performances even if the NLI model is conservative. Furthermore, we think that a critical parameter is represented by the input connector loss as its value has been assumed and it determines the amount of NLI introduced by each fiber span and thus, the estimated GSNR.

## 5. CONCLUSIONS AND NEXT STEPS

We presented the GNPy for the physical layer abstraction of optical networks by describing the general structure, the functionalities and its core structure, also, by describing the scientific bases. Then, we delineated the validation procedure of the QoT-E and this can be, in general, followed to use GNPy on any real network to predict the QoT of a lightpath. Later, we described the test-bed we used and we compared the estimated GSNR against the measured values. We showed that, following a procedure that relies only on the data obtained by querying the network equipment and the data present in the equipment documentation, it is possible to obtain excellent accuracy. In our measurement, the error is within 1 dB in 90% of cases on a sample size of 500 measurements. Furthermore, we showed that GNPy is able to predict the optimum transmitted power with good accuracy – within 0.5 dB – and thus, it can be used in an optical line controller to compute the optimum working point. This validation was carried out with excellent results by varying the paths' distances, the modulation format and the configuration of the network, and by probing C-band on different spectral areas to show the ability of the QoT-E to predict the frequency variation of the GSNR. Moreover, the capability of tracking variations in the amplifiers setup demonstrates that GNPy is suitable as an engine for a what-if framework. Then, an initial step in validating the goodness in predicting the performances of Raman amplification has been demonstrated. Additional testing with focus on longer fiber spans and even higher distribution of hybrid or Raman amplification will serve as valuable source of test data. Another further step, so far missing, is a brown field validation, to test the accuracy in the presence of environmental and aging issues. In a brown field scenario, in fact, many splices are present along the fibers because of the continuous fiber cuts and the connectors may be not perfectly cleaned.

## ACKNOWLEDGMENTS

GNPy has been developed by the PSE-OOPT working group within the Telecom Infra Project.

## REFERENCES

1. "TIP Open Optical & Packet Transport (OOPT)," https://telecominfraproject.com/oopt/.
2. "GitHub repository of GNPy," https://github.com/Telecominfraproject/oopt-gnpy.
3. V. Kamalov, M. Cantono, V. Vusirikala, L. Jovanovski, M. Salsi, A. Pilipetskii, D. K. M. Bolshtyansky, G. Mohs, E. R. Hartling, and S. Grubb, "The subsea fiber as a Shannon channel," in *In Proceedings of the SubOptic,* (2019).
4. I. Busi and S. Belotti, "YANG model for requesting path computation," Internet-Draft `draft-ietf-teas-yang-path-computation-06`, Internet Engineering Task Force (2019). Work in Progress.
5. V. Curri, A. Carena, A. Arduino, G. Bosco, P. Poggiolini, A. Nespola, and F. Forghieri, "Design strategies and merit of system parameters for uniform uncompensated links supporting nyquist-wdm transmission," J. Light. Technol. **33**, 3921–3932 (2015).
6. A. Ferrari, M. Cantono, U. Waheed, A. Ahmad, and V. Curri, "Networking benefits of advanced dsp techniques and hybrid fiber amplification," in *2017 19th International Conference on Transparent Optical Networks (ICTON),* (IEEE, 2017), pp. 1–4.
7. A. Ferrari, D. Pilori, E. Virgillito, and V. Curri, "Power control strategies in C+ L optical line systems," in *Optical Fiber Communication Conference,* (Optical Society of America, 2019), pp. W2A–48.

8. V. Curri, M. Cantono, and R. Gaudino, "Elastic all-optical networks: A new paradigm enabled by the physical layer. how to optimize network performances?" J. Light. Technol. **35**, 1211–1221 (2017).
9. B. D. Taylor, G. Goldfarb, S. Bandyopadhyay, V. Curri, and H.-J. Schmidtke, "Towards a route planning tool for open optical networks in the telecom infrastructure project," in *Optical Fiber Communication Conference,* (Optical Society of America, 2018), pp. Tu3E–4.
10. M. Filer, M. Cantono, A. Ferrari, G. Grammel, G. Galimberti, and V. Curri, "Multi-vendor experimental validation of an open source QoT estimator for optical networks," J. Light. Technol. **36**, 3073–3082 (2018).
11. A. Ferrari, M. Filer, K. Balasubramanian, Y. Yin, E. LeRouzic, J. Kundrát, G. Grammel, G. Galimberti, and V. Curri, "Experimental validation of an open source quality of transmission estimator for open optical networks," in *2020 Optical Fiber Communications Conference and Exhibition (OFC),* (IEEE, 2020), p. W3C.2.
12. J.-L. Auge, V. Curri, and E. L. Rouzic, "Open design for multi-vendor optical networks," in *Optical Fiber Communication Conference (OFC) 2019,* (Optical Society of America, 2019), p. Th1I.2.
13. J. Kundrát, O. Havliš, J. Jedlinský, and J. Vojtěch, "Opening up ROADMs: Let us build a disaggregated open optical line system," J. Light. Technol. **37**, 4041–4051 (2019).
14. "Exchange with GNPy to check path feasibility," https://git.opendaylight.org/gerrit/c/transportpce/+/81785.
15. A. Ferrari, A. Tanzi, S. Piciaccia, G. Galimberti, and V. Curri, "Selection of amplifier upgrades addressed by quality of transmission and routing space," in *2019 Optical Fiber Communications Conference and Exhibition (OFC),* (IEEE, 2019), pp. 1–3.
16. M. Cantono, D. Pilori, A. Ferrari, C. Catanese, J. Thouras, J.-L. Augé, and V. Curri, "On the interplay of nonlinear interference generation with stimulated Raman scattering for QoT estimation," J. Light. Technol. **36**, 3131–3141 (2018).
17. M. Cantono, A. Ferrari, D. Pilori, E. Virgillito, J. Augé, and V. Curri, "Physical layer performance of multi-band optical line systems using Raman amplification," J. Opt. Commun. Netw. **11**, A103–A110 (2019).
18. I. Roberts, J. M. Kahn, J. Harley, and D. W. Boertjes, "Channel Power Optimization of WDM Systems Following Gaussian Noise Nonlinearity Model in Presence of Stimulated Raman Scattering," J. Light. Technol. **35**, 5237–5249 (2017).
19. D. Semrau, R. I. Killey, and P. Bayvel, "The Gaussian noise model in the presence of inter-channel stimulated raman scattering," J. Light. Technol. **36**, 3046–3055 (2018).
20. J. Bromage, "Raman amplification for fiber communications systems," J. Light. Technol. **22**, 79 (2004).
21. A. Carena, G. Bosco, V. Curri, Y. Jiang, P. Poggiolini, and F. Forghieri, "EGN model of non-linear fiber propagation," Opt. express **22**, 16335–16362 (2014).
22. F. Zhang, Q. Zhuge, and D. V. Plant, "Fast analytical evaluation of fiber nonlinear noise variance in mesh optical networks," IEEE/OSA J. Opt. Commun. Netw. **9**, C88–C97 (2017).
23. R. T. Fielding and R. N. Taylor, *Architectural styles and the design of network-based software architectures*, vol. 7 (University of California, Irvine Doctoral dissertation, 2000).
24. R. Enns, M. Bjorklund, J. Schoenwaelder, and A. Bierman, "RFC 6241, network configuration protocol (NETCONF)," Internet Eng. Task Force (IETF), June (2011).
25. M. A. Taubenblatt, "Optical interconnects for high-performance computing," J. Light. Technol. **30**, 448–457 (2011).
26. A. Ferrari, M. Cantono, B. Mirkhanzadeh, Z. Lu, A. Shakeri, C. Shao, M. Tacca, M. Razo, A. Fumagalli, G. Martinelli *et al.*, "A two-layer network solution for reliable and efficient host-to-host transfer of big data," in *2018 20th International Conference on Transparent Optical Networks (ICTON),* (IEEE, 2018), pp. 1–4.
27. D. Derickson, C. Hentschel, and J. Vobis, *Fiber optic test and measurement*, vol. 8 (Prentice Hall PTR New Jersey, 1998).
28. V. Curri and A. Carena, "Merit of Raman pumping in uniform and uncompensated links supporting nywdm transmission," J. Light. Technol. **34**, 554–565 (2015).
29. D. J. Elson, G. Saavedra, K. Shi, D. Semrau, L. Galdino, R. Killey, B. C. Thomsen, and P. Bayvel, "Investigation of bandwidth loading in optical fibre transmission using amplified spontaneous emission noise," Opt. express **25**, 19529–19537 (2017).
30. P. Poggiolini, G. Bosco, A. Carena, R. Cigliutti, V. Curri, F. Forghieri, R. Pastorelli, and S. Piciaccia, "The LOGON strategy for low-complexity control plane implementation in new-generation flexible networks," in *2013 Optical Fiber Communication Conference and Exposition and the National Fiber Optic Engineers Conference (OFC/NFOEC),* (IEEE, 2013), pp. 1–3.